Biophysical Journal
Article

Biophysical Society

Actin-Regulator Feedback Interactions during Endocytosis

Xinxin Wang,[1] Brian J. Galletta,[2] John A. Cooper,[3] and Anders E. Carlsson[1,*]
[1]Department of Physics, Washington University, St. Louis, Missouri; [2]Cell Biology and Physiology Center, National Heart, Lung, and Blood Institute, National Institutes of Health, Bethesda, Maryland; and [3]Department of Cell Biology and Physiology, Washington University School of Medicine, St Louis, Missouri

ABSTRACT Endocytosis mediated by clathrin, a cellular process by which cells internalize membrane receptors and their extracellular ligands, is an important component of cell signaling regulation. Actin polymerization is involved in endocytosis in varying degrees depending on the cellular context. In yeast, clathrin-mediated endocytosis requires a pulse of polymerized actin and its regulators, which recruit and activate the Arp2/3 complex. In this article, we seek to identify the main protein-protein interactions that 1) cause actin and its regulators to appear in pulses, and 2) determine the effects of key mutations and drug treatments on actin and regulator assembly. We perform a joint modeling/experimental study of actin and regulator dynamics during endocytosis in the budding yeast *Saccharomyces cerevisiae*. We treat both a stochastic model that grows an explicit three-dimensional actin network, and a simpler two-variable Fitzhugh-Nagumo type model. The models include a negative-feedback interaction of F-actin onto the Arp2/3 regulators. Both models explain the pulse time courses and the effects of interventions on actin polymerization: the surprising increase in the peak F-actin count caused by reduced regulator branching activity, the increase in F-actin resulting from slowing of actin disassembly, and the increased Arp2/3 regulator lifetime resulting from latrunculin treatment. In addition, they predict that decreases in the regulator branching activity lead to increases in accumulation of regulators, and we confirmed this prediction with experiments on yeast harboring mutations in the Arp2/3 regulators, using quantitative fluorescence microscopy. Our experimental measurements suggest that the regulators act quasi-independently, in the sense that accumulation of a particular regulator is most strongly affected by mutations of that regulator, as opposed to the others.

INTRODUCTION

Endocytosis encompasses a set of engulfment processes by which cells absorb molecules and materials from outside the cell (1). The clathrin-mediated form of endocytosis (CME), in which membrane invaginations are surrounded by clathrin coats, is used by the cell for multiple purposes, including the regulation of plasma membrane activities and the ingestion of essential nutrients. In addition to its importance for cellular functions, CME provides an attractive system to study membrane deformation by actin and other cytoskeletal and membrane-associated proteins. Actin polymerization often plays an important role in CME. In yeast, CME requires actin polymerization (2,3). In mammalian cells, the role of actin polymerization depends on the physical conditions. When membrane tension is high, the requirement for actin polymerization is more stringent (4).

These findings motivate the study of actin polymerization dynamics during CME. Yeast is an attractive system for CME because of the ease of genetic manipulation, and the ability to perform live-cell imaging of fluorescent fusion proteins, expressed at endogenous levels. Actin polymerization and depolymerization during CME occur as part of the assembly and disassembly of a protein patch containing >60 different proteins, arriving in a well-defined sequence (5,6). Initially cargo and adaptor proteins assemble, followed by a coat including clathrin and other proteins. The coat recruits actin regulators, sometimes referred to as "nucleation promoting factors". The regulators, including Las17 (yeast WASP), Myo3, Myo5 (yeast class-1 myosins), and Pan1 (an Eps15-like protein) in budding yeast, recruit and activate the Arp2/3 complex to nucleate new actin filaments from the side of existing filaments. After actin polymerization begins, membrane bending occurs (7), and a tubule forms and it eventually pinches off into a vesicle, followed ultimately by dissolution of the protein coat.

Submitted September 23, 2015, and accepted for publication February 8, 2016.

*Correspondence: aec@wustl.edu

Editor: David Odde.
http://dx.doi.org/10.1016/j.bpj.2016.02.018

Several studies have measured the effects of perturbations on the assembly of actin and its regulators in yeast. The actin inhibitor latrunculin (5) extended the lifetime of coat proteins, while the Arp2/3 inhibitor CK-666 (8) extended the actin lifetime and decreased the number of actin patches. Deletions of the gene encoding the endocytic coat protein Sla2 (9,10) resulted in the formation of comet-shaped actin structures extending inwards from the cell cortex. We measured the effects of mutations affecting the budding yeast Arp2/3 regulators Las17, Myo3, Myo5, and Pan1, on the numbers of copies of actin and actin-binding proteins at the endocytic site (11). These mutants had truncations of regulator acidic domains, which bind and activate Arp2/3 complex; so we expected less activation of Arp2/3 and decreased F-actin. However, the acidic-domain truncations did not significantly reduce the maximum F-actin count, and in some mutants it unexpectedly increased. A preliminary mathematical model suggested that a negative-feedback interaction between F-actin and the Arp2/3 regulators might contribute to this effect.

Two modeling studies in the literature have addressed the dynamics of F-actin in CME protein patches. One study, in budding yeast, treated a mechanism for protein pulse generation, based on indirect negative feedback interactions acting on the regulators, including the effects of membrane deformation and PIP2 hydrolysis (12). This model explained several traits of endocytosis mutants. A second study, in fission yeast, treated a multistep model of actin filament nucleation, growth, and capping, based on an assumed time course for the active Arp2/3 regulator (13). It provided important insights into the kinetics of cellular processes relative to those observed in vitro, and highlighted the role of severing in actin disassembly.

In this article, we seek to establish the main protein interactions that drive actin and regulator pulse dynamics in wild-type cells, and determine the effects of mutations and drug treatments on actin polymerization. To this end, we combine stochastic modeling studies of actin polymerization with a negative-feedback interaction between F-actin and the membrane. The model provides a more detailed treatment of the actin network than the models in the previous two studies (12,13), because the network is explicitly grown in three dimensions. The effects of force on filament growth and branching are also included in a physically consistent fashion.

We find that our stochastic-growth/negative-feedback model explains key effects of the mutations and drug treatments discussed above. It also predicts an increase of regulator count under the conditions of reduced branching resulting from acidic-domain mutations of the regulators. This prediction is reinforced by results from a simple two-variable rate-equation model of the regulator/actin dynamics. We test the prediction by measuring the regulator counts in mutated yeast cells using fluorescence microscopy, and the experiments confirm the prediction.

MATERIALS AND METHODS

Fluorescence imaging experiments

To test the predictions of the theoretical models, we measured the effects of acidic-domain mutations on the regulator counts. We extended our previous measurements of Abp1, capping protein, and Arp2/3 complex (11) to measure the counts of the four regulators Las17, Pan1, Myo3, and Myo5 in wild-type cells and the following mutants: *las17*Δ*acidic*; *pan1*Δ*acidic*; *myo5*Δ*acidic*; *myo3*Δ*acidic myo5*Δ*acidic*; *las17*Δ*acidic pan1*Δ*acidic*; and *myo3*Δ*acidic myo5*Δ*acidic pan1*Δ*acidic*. We also reanalyzed our Abp1 data (11), which had previously been analyzed using different software. These measurements allow us to test our predictions of the effects of mutations on regulator counts, and provide a database for fitting the models. Our measurements of the cross effects of mutation of one regulator on assembly of another regulator also allow us to ascertain the effects of interactions between regulators on their assembly. Our methods for generating yeast strains, as well as the microscopy and image analysis, are similar to those in Galletta et al. (11). We give more information about these methods, and the protein counting methods, in the Supporting Material.

RESULTS

Mathematical models

The models treat the dynamics of actin polymerization and the regulator Las17, the yeast form of Wiskott-Aldrich syndrome protein (WASP). We focus on Las17 because the in vitro experiments (14) suggest that it has the strongest nucleation activity. Furthermore, the other regulators with strong nucleation activity, class-1 myosins Myo3 and Myo5, have a motor activity that is beyond this analysis. Treating Las17 by itself is certainly an approximation, but our data (see Fluorescence Imaging Experiments, below) suggest that to some extent the regulators act independently of each other. We define L as the number of Las17 molecules in the endocytic protein patch.

The models extend our preliminary negative-feedback model (11). They share the following main assumptions:

1) L grows by an autocatalytic self-assembly mechanism (see Box *A* of Fig. 1) from an initial fluctuation of magnitude L_0. In the absence of polymerized actin, L approaches a plateau value at long times. Autocatalytic self-assembly would result from indirect or direct attractive interactions between Las17 monomers. Such interactions have been demonstrated by in vitro experiments (15,16) showing that WASP, in combination with adaptor proteins, self-assembles up to a certain limiting concentration.

We do not include actin-dependent terms in the assembly rate for two reasons: first, Las17 patches in budding and fission yeast assemble in the absence of polymerized actin (9,17-19), and second, Las17 assembles for a period of ~20 s before actin arrives at the patch. In fission yeast, treatment with latrunculin (18), which inhibits actin polymerization, and mutation of cofilin (19), which severs actin filaments, slows the accumulation of Wsp1. This suggests

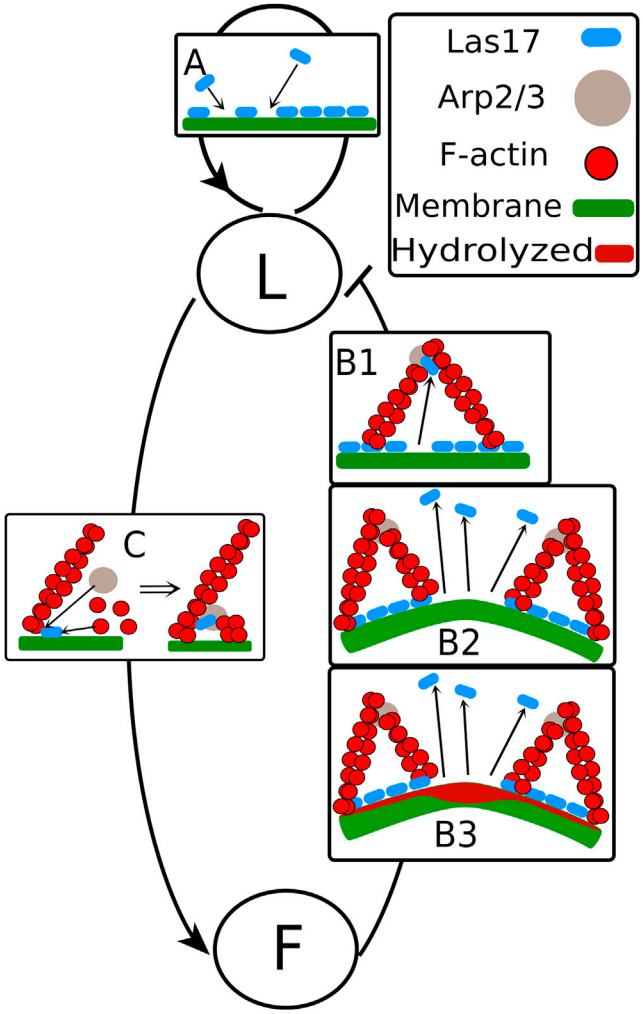

FIGURE 1 Schematic of modeled protein interactions. *L* is Las17 and *F* is F-actin. (*Blue ovals*) Las17. (*Gray circles*) Arp2/3 complex. (*Red circles*) Actin monomers. Membrane is green and region where PIP2 is hydrolyzed is dark red. Box *A* shows the self-recruitment of Las17. Boxes *B1–B3* show possible mechanisms for the negative feedback of F-actin on Las17. Box *C* shows how Las17, Arp2/3 complex, and actin monomers enter the branching mechanism. To see this figure in color, go online.

feedback of F-actin onto Wsp1 assembly. We are not aware of such an effect in budding yeast; furthermore, the rapid assembly of Wsp1 compared to Las17 suggests that the underlying biophysical mechanisms may be quite different. This is consistent with the large evolutionary distance between the organisms.

2) The disassembly of regulators is accelerated by actin polymerization, leading to a negative feedback effect. Negative feedback between actin and Arp2/3 regulators is suggested by several observations. First, the regulator time courses during endocytosis have the form of a pulse, and this pulse lifetime is extended by latrunculin, which inhibits actin polymerization (9,20). Second, in mammalian cells, latrunculin slows the membrane dynamics of WAVE complex, another Arp2/3 regulator (21,22). Finally, traveling waves of F-actin along the plasma membrane have been observed in several cell types, and theoretical models have found it necessary to assume negative feedback effects to explain these phenomena (see Allard and Mogilner (23) for a review). Without a negative-feedback term, none of our models is able to obtain the pulse behavior of the proteins. A similar negative-feedback effect between polymerized actin and coat proteins has been suggested previously (12,19).

At least three physical mechanisms could mediate this negative-feedback effect. In Fig. 1, box *B1*, newly nucleated filaments pull Las17 off the membrane, after which Las17 diffuses into the cytoplasm. The actin filament network moves away from the membrane, so this process could result from the binding of Las17 to Arp2/3 complex in the actin network, or to the actin network itself. The WH2 domain of the actin regulator N-WASP binds to actin (24). Because Las17 also has a WH2 domain, it could bind F-actin.

We note that, in Arp2/3 branching studies using a di-VCA WASP fragment, most di-VCA molecules detached from the mother filament before the new branch was generated (25). If Las17 detaches in a similar fashion, the newly nucleated filament will not pull Las17 with it. However, the resolution of the experiment was such that the number of di-VCA molecules staying on filaments (Fig. 2D of Smith et al. (25)) could be up to 40% of the number of filaments forming. Our stochastic model, which assumes that 10% of branching events cause Las17 detachments, is thus consistent with Smith et al. (25). Furthermore, Las17 has a polyproline actin-binding domain (26) that is not present in di-VCA. This domain might allow new actin branches to drag Las17 off the membrane.

In Fig. 1, box *B2*, curvature or tension of the membrane, generated by actin polymerization, weakens the binding of Las17 or the underlying coat proteins to the membrane (12). This mechanism is supported by studies revealing tension-dependent binding of clathrin (27) and the WASP-binding protein FBP17 (28) to membranes, and the curvature-dependent binding of the regulator WASP to vesicles (29).

In Fig. 1, box *B3*, membrane curvature, or proteins recruited by polymerized actin, hydrolyze PIP2, which in turn weakens the binding of the coat proteins and regulators to the membrane (12). This hypothesis is supported by the finding that recruitment to actin patches of the synaptojanin Sjl2, which hydrolyzes PIP2 (30), is dependent on F-actin (31). Furthermore, PIP2 hydrolysis depends on membrane curvature (32).

3) Actin filament nucleation is autocatalytic, so that preexisting actin filaments accelerate polymerization (see Box *C* in Fig. 1). This assumption is based on the branching nature of Arp2/3-induced actin filament nucleation,

where Arp2/3 nucleates new filaments by binding to the sides of existing filaments (33,34).

The applicability of a model treating spontaneous (non-branching) nucleation is discussed in the Supporting Material. To enhance the robustness of our results, we perform two types of model calculations, stochastic-growth and rate-equation. The stochastic-growth calculations generate an explicit actin network in three dimensions. This network interacts with the actin regulators at the cell membrane, and its growth is slowed by opposing force. The rate-equation models capture the key features of the stochastic-growth calculations in a compact form.

Stochastic-growth model

This model is similar to the model used by one of us to study F-actin waves in animal cells (35), and it shares general features with several other models of actin waves (21,36-38). It uses a Monte Carlo-type network-growth methodology as in Carlsson (39). Polymerization, branching, capping, and network disassembly are treated as stochastic events described by rate parameters k_{on}, k_{br}, k_{cap}, and k_{sev}. The network is assumed rigid, and it moves away from the membrane at a rate determined by the polymerization rate of the filaments in contact with the membrane. Network disassembly is assumed to occur by the disappearance of entire filaments, one at a time. We neglect the possibility of reattachment of filaments to the network. Previous work (13) has shown that actin dynamics in fission yeast is well described without including reattachment. Details are given in the Supporting Material.

The geometry of the model and its forces (Fig. 2) are based on the explicit mechanical calculations of Carlsson and Bayly (40), and on theories (2,41,42) in which retrograde flow of actin drives invagination by pulling the region inwards. The regulators are uniformly distributed on the membrane on a ring with an inner radius of 25 nm and an outer radius of 75 nm (Fig. 3), corresponding roughly to the radii of the invagination and the actin polymerization zone found in Kukulski et al. (7). The assumed distribution is consistent with observed rings of the protein Sla1 (6), F-actin rings during CME in COS-7 cells (43), and with experimental observations of membrane localization of Las17 (6,9,44). (We note, however, that a small, <100 nm, small inward motion of Las17 has been suggested (6).) We assume that the regulators redistribute rapidly in the Las17 region. This is plausible because the turnover times for the regulator N-WASP on viruses (45) and clathrin in mammalian cells (46) are only ~2 s (45). Therefore, we treat a uniform distribution of Las17 molecules rather than specifying individual coordinates.

We base our description of regulator assembly on a simple reaction-rate theory. If the Las17 assembles by interaction of a molecule in solution with a pair of molecules bound to the membrane, and the concentration in solution is regarded as constant on the assumption that diffusion is rapid, then the assembly rate will be proportional to L^2 (47). If the reaction occurs in a fixed region where each Las17 molecule takes up a certain area, the number of sites available for reaction will be reduced by a factor proportional to $L_2 - L$, where L_2 is the maximum number of molecules that can fit. Combining these dependences, we obtain an assembly rate proportional to $L^2(L_2 - L)$, and we use this in the bulk of the calculations. Interactions of different orders correspond to different powers in this expression. We have found that assembly rates proportional to $L(L_2 - L)$ and $L^3(L_2 - L)$ preserve the basic predictions of the model. However, an assembly rate proportional to $(L_2 - L)$, which

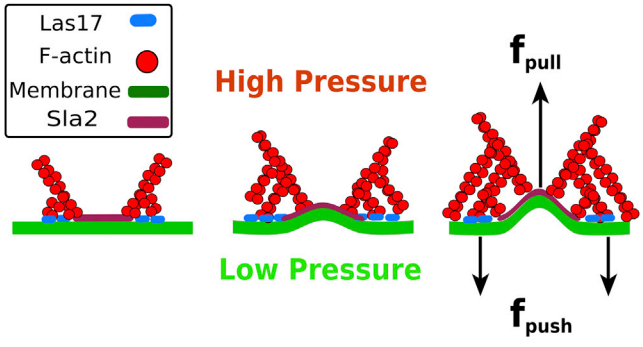

FIGURE 2 Schematic of the 3D geometry of the stochastic-growth model. Actin filaments polymerizing from a ring of Las17 push against the membrane, pulling other filaments attached to Sla2 at the membrane back with them. The osmotic pressure is higher in the interior (*up arrow*), and the force of actin polymerization helps overcome this pressure difference. The turgor pressure is the difference between the interior and exterior osmotic pressures. To see this figure in color, go online.

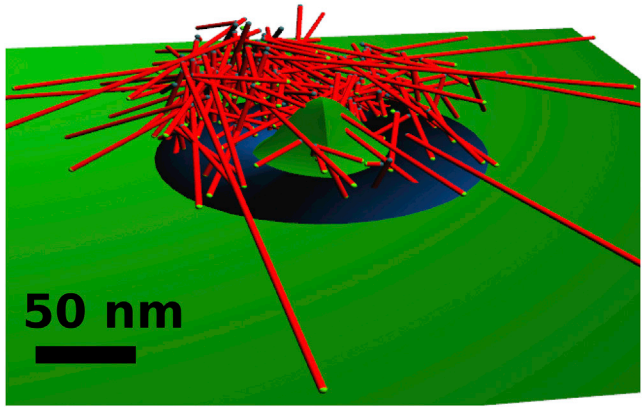

FIGURE 3 Oblique snapshot of the stochastic simulation geometry, after 23 s of a wild-type simulation run. Actin filaments are red cylinders, with barbed ends in light green spheres; the membrane is green. The blue disk around the center represents the Las17 region where actin filament branches form. The membrane profile is not explicitly treated by the model but we include an approximation to it to clarify the physical picture. We assumed that the membrane deformation at the center is the average distance from the actin filament pointed ends to the membrane, provided that the number of filaments and the F-actin count exceed the threshold value for force generation (see text). The width of the deformation corresponds roughly to known invagination widths (7). To see this figure in color, go online.

does not contain an autocatalytic term, gives poor results for both wild-type and mutant cells (see the Supporting Material). We thus use an average rate of $k_0L^2(L_2 - L)$, where k_0 is a rate parameter. The process is treated stochastically.

The polymerization rate is $k_{on}G$, where G is the free-actin concentration, and the branching rate per subunit is $k_{br}L$. Branching is assumed to occur only in a donut-shaped region above the regulator ring, within a branching width $W = 20$ subunits $= 54$ nm of the membrane. We implement the negative feedback of F-actin on Las17 by assuming that a Las17 molecule can leave the membrane (and become inactive), with probability α, when a branching nucleation event occurs. This corresponds to mechanism *B1* in Fig. 1. The Las17 molecules are assumed to detach from the actin network when they leave the membrane, because Las17 moves inward much less than the actin network (6,9).

The main model does not treat membrane deformation explicitly, for reasons of computational practicality. We still feel that the results are meaningful, because the main actin regulators remain near the membrane during invagination (6,9,44). In the Supporting Material we describe a model in which regulator detachment is driven by membrane deformation rather than by branching dynamics, corresponding to mechanisms *B2* and *B3* in Fig. 1. We were unable to obtain physically reasonable results with this model.

We treat the forces opposing actin network growth in a simplified fashion (Fig. 2). Because the viscous drag on the actin network is extremely small, we assume a balance of forces on the network leading to zero net force. In the outer region of the network, defined by the Las17 ring, the filaments push against the membrane, and thus experience a force opposing their growth. The inner region of the network pulls on the membrane via linker proteins such as Sla2. The magnitude of the pushing force opposing actin polymerization in the ring is equal to the magnitude of the pulling force.

The dominant opposing force that must be overcome in the pulling region likely results from turgor pressure (40,48). Estimates of the turgor pressure in budding yeast vary widely, from 0.05 MPa (49) to roughly 0.6 MPa (50); in fission yeast a higher value of 0.85 MPa has been measured (51). If one assumes a radius of 25 nm (7) for the pulling region, the total estimated force for budding yeast then ranges from 100 to 1200 pN. We define f_a as the portion of the total force that needs to be overcome by actin polymerization, and we assume that the remaining force is supplied by curvature-generating proteins such as clathrin and BAR-domain proteins. The value of f_a is highly uncertain. We used a value of 415 pN, approximately one-third of the highest value of the total force. The results were insensitive to the value of f_a (see the Supporting Material).

We treat the slowing of actin polymerization by f_a by assuming that a critical minimum number of filaments and subunits (taken to be 20 and 200, respectively) is required to form a continuous network that can exert a pulling force on the membrane. When these critical numbers are not reached, there is no opposing force. When the critical numbers are reached, then the network experiences the force f_a. We take the on-rate for the free filaments touching the membrane to have the familiar Brownian-ratchet form (52):

$$k_{on}^{touch} = k_{on}\exp(-f_a\delta/N_{touch}k_BT), \quad (1)$$

where N_{touch} is defined as the number of filaments within two subunits of the membrane. In principle, the on-rate in Eq. 1 should include cosine factors depending on the filament orientation. We found that the inclusion of such factors gives results similar to lowering f_a, so we decided to use the simpler form of Eq. 1. The retrograde velocity of the actin network is then given by $k_{on}^{touch}\delta\langle\cos\theta\rangle$, where $\delta = 2.7$ nm is the length added per subunit, θ is the orientation angle of a filament, and the average is taken over the touching filaments.

We parameterize the model for budding yeast. The model's potential relevance to fission yeast is described in the Discussion. The key parameters in the model are $k_{on}G$, k_{br}, k_{cap}, k_{sev}, k_0, and α, whose values and definitions are given in Table 1. Because error minimization with the stochastic-growth code is computationally demanding, we obtained an initial parameter set using a faster four-variable rate-equation code (see the Supporting Material), and performed further optimization using the stochastic code. The optimization with the stochastic code was accelerated by the use of a graphical processing unit together with the CUDA programming language (53). To avoid overfitting, we do not vary all of these parameters, but rather assign a k_{cap} a fixed value, from the four-variable model. The remaining five parameters, $k_{on}G$, k_{br}, k_{sev}, k_0, and α, were obtained by a least-squares fit to the following six properties of the time courses: the peak heights of L and F; the full widths at half-maximum of the time courses of L and F; and the

TABLE 1 Parameters and Initial Values for Stochastic and Rate-Equation Models

Model	Stochastic	Rate Equation
Parameters		
$k_{on}G$, barbed-end on-rate (s^{-1})	32	—
k_{br}, subunit branching rate (10^{-3} s^{-1})	2.17	0.957
k_{cap}, capping rate (s^{-1})	0.667	—
k_{sev}, severing rate (s^{-1})	0.300	0.427
W, branching layer thickness (nm)	54	—
f_a, total actin-membrane force (pN)	415	—
k_0, Las17 assembly rate constant (10^{-5} s^{-1})	3.5	3.93
α, Las17 detachment probability	0.100	0.136
$\bar{l}$, average filament length in subunits	—	30
L_2, maximum Las17 count	101	101
k_{nuc}, filament nucleation rate (10^{-2} s^{-1})	2	—
Initial values		
L_0, Las17 count	20	18
N_0, number of filaments	5	—
F_0, F-actin count	100	1

peak counts of capping protein and Arp2/3 complex taken from our previous work (11). Note that the fitted value of α is small, suggesting that most Las17 molecules remain on the membrane during branching events.

The simulation begins with five primer actin filaments (54) placed with random positions and orientations in the Las17 disk, and a starting value of $L_0 = 20$ Las17 molecules. The value of L_0 was chosen with two considerations in mind: 1) the critical nucleus is probably relatively large, to prevent very rapid nucleation of patches; and 2) L_0 should be much smaller than L_2. Primer filaments are also produced at a low continuing rate of 0.02 s^{-1}. The simulations were run 2000 times for each parameter set to obtain meaningful averages. Because several of the parameters and functional dependences are uncertain, we varied parameters and assumptions to see the effects on the model predictions (see the Supporting Material).

The actin patch lifecycle illustrated in the representative snapshots of Fig. 4 *a* has the following three steps: initiation from primer filaments; rapid polymerization via branching nucleation; and, finally, depolymerization as regulators are removed and inactivated. Fig. 5 *a* compares the predicted wild-type time courses with our experimental data (more complete data is given under Fluorescence Imaging Experiments). The predicted time courses are similar to the experimental ones, and also to previously published ones (6,14). Because we do not have a direct measurement of the F-actin count, we estimate the measured F in this and following figures as 8.9 times the measured Abp1 count, which results from assuming a value of 6000 for the wild-type peak value of F (34); dividing this by our measured peak wild-type value of 674 (see Fluorescence Imaging Experiments) for Abp1 gives the factor of 8.9. Because we did not perform two-color experiments, we could not measure the delay between the Las17 peak and the actin polymerization peak. Therefore, in presenting our data and corresponding model results, we do not show the delay, but rather align all of the time courses at their maxima. The delay in our model results is a few seconds, consistent with previous results using two-color imaging (6,14). Because several of the processes treated in the model are stochastic, a substantial degree of asymmetry is often seen in the actin patches (see Fig. 3), reminiscent of the asymmetry seen in electron micrographs of CME in mammalian cells (55).

Modeling effects of mutations and drug treatments on cells

To further explore the relevance of this model to the experimental system, we have studied four interventions in silico, whose effects on cells have been measured in vivo:

Mutations of the acidic Arp2/3-binding regions of Las17. The acidic A-regions of the regulators are believed to be important for nucleation because they bind Arp2/3 complex. In vitro studies (56) have also shown that these domains (as well as the combination of these domains with WH2 domains, called "WA") can activate the Arp2/3 complex. We thus model the A-region mutations by reducing k_{br}. We do not know how large the reduction is. In vitro data (57) for WASP suggest that the A-region mutation renders Las17 completely inactive ($k_{br} = 0$). However, our previous observation (11) of a substantial F-actin count even in cells containing A-region mutations of the three nucleators believed to be the strongest, Las17, Myo3, and Myo5, suggests that k_{br} is not driven to zero by these mutations. A nonzero value of k_{br} could be caused by either 1) intrinsic activity of the

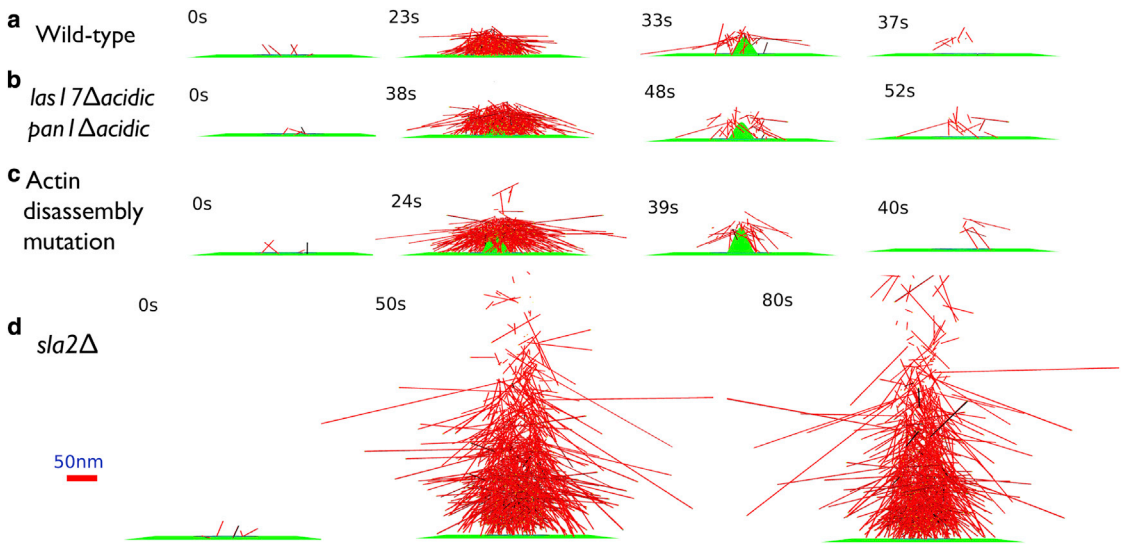

FIGURE 4 Side-view snapshots of stochastic simulations for different interventions. Color conventions are as in Fig. 3. Each of the rows (*a–c*) shows the initiation of the simulation, the F-actin peak, disassembly, and near disappearance. Row (*d*) shows the initial phase and later time points where the F-actin count reaches a steady state. The membrane profile is approximated as in Fig. 3, except that in row (*d*) we assumed that the actin gel was unable to pull on the membrane. To see this figure in color, go online.

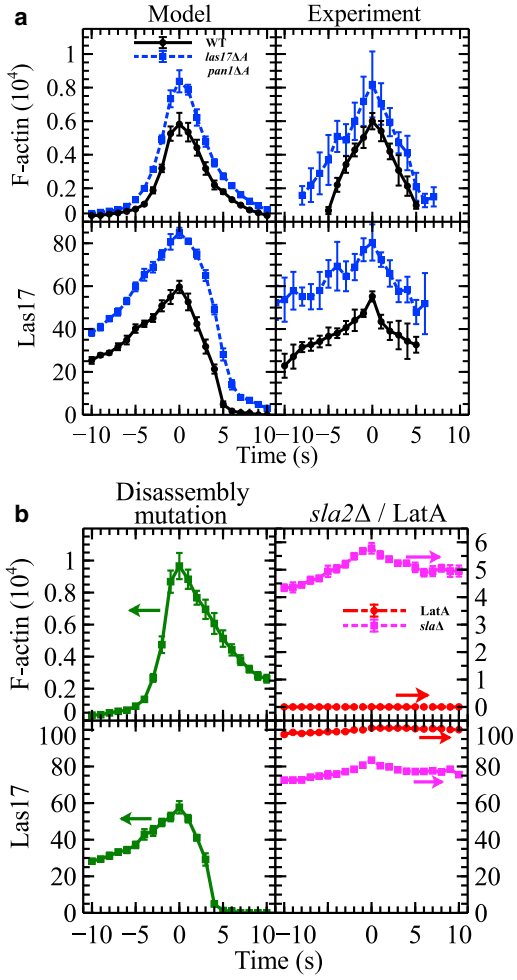

FIGURE 5 Time courses of L and F from stochastic simulations and experiments (described in detail under Fluorescence Imaging Experiments). (*a*) Wild-type and *las17*Δacidic *pan1*Δ*acidic* mutant, (*b*) disassembly mutant, *sla2*Δ mutant, and LatA-treated cells. F-actin count is a measured Abp1 count multiplied by a conversion factor of 8.9 (see text). Model results obtained from 2000 simulation runs, displayed in the same way as the experimental data (see the Supporting Material): plotted points correspond to mode values; error bars are the standard deviation of a distribution of 1000 mode values obtained by bootstrapping. The time courses in this and subsequent figures are aligned with their peaks at time $t = 0$. Arrows in frame (*b*) indicate which vertical scale to read. To see this figure in color, go online.

Arp2/3 complex (requiring recruitment but not activation) (58); 2) branching activity of other nucleators; or 3) nucleation activity of Las17 not requiring the A-region (34).

In the absence of a negative-feedback interaction, acidic-domain mutations would cause a large reduction in the F-actin peak count F_{max}, roughly proportional to the reduction in k_{br}. Our simulations including negative feedback show a qualitatively different behavior. When k_{br} is reduced by fractions up to 70%, F_{max} increases rather than dropping proportionally to k_{br}. When k_{br} is reduced by >70%, F_{max} is reduced, and F_{max} equals the initial F value when $k_{br} = 0$. Figs. 4 *b* and 5 *a* show model results for a 40% reduction in k_{br}, along with the corresponding experimental data. The simulations predict a 40% increase in F_{max}, consistent with the data, and our previous experimental findings (11) for cells with single acidic-domain mutations of Las17 and cells with acidic-domain mutations of both Las17 and Pan1. The magnitude of the predicted effect, for this value of k_{br}, is comparable to the measured one for the double mutant, and we label the figure frames accordingly.

The simulations also predict an increase in the peak Las17 count L_{max}, of ~40%, which is confirmed by our data (Fig. 5 *a*). The increase occurs in the model because the reduced branching rate leads to less Las17 being pulled off the membrane. The increase in L_{max} in turn causes the increase in L_{max}, which is determined by a competition between the increased amount of Las17 present and the reduced k_{br}. The prediction of increased L_{max} is very robust: L_{max} always increases when k_{br} is decreased, and the increase is a monotonic function of k_{br}.

Disassembly mutations. We model mutations that slow actin disassembly by reducing k_{sev}. Actin disassembly is believed to be delayed relative to actin assembly because it follows hydrolysis of ATP on F-actin. This belief is supported by the observations that assembly of cofilin, which accelerates actin disassembly, is delayed relative to F-actin (19,59). Therefore, we model actin disassembly mutations as a decrease in k_{sev} that occurs after a delay. For computational convenience, the delay is described in terms of a minimum number of filaments (100) that must be reached before k_{sev} is decreased. Actin disassembly mutants that have been studied in budding yeast include the actin *act1-159* mutation (60), which delays disassembly because a conformational change is prevented, and the *cof1-22* cofilin mutation (59,61,62). We do not know how large the reduction in k_{sev} is for a given mutation, and we show results for a reduction of 50% in Figs. 4 *c* and 5 *b*. The model predicts that F_{max} is increased by ~60%; the F-actin lifetime is greatly increased; and the regulator count is decreased by cofilin mutation. The predictions for F-actin are qualitatively consistent with the findings that actin patches in budding yeast are 25% brighter in *act1-159* mutant cells (60), and that their disassembly is delayed in both the *act1-159* and *cof1-22* mutants (59,61,62).

Sla2 deletion. Sla2 couples actin polymerization to membrane deformation (63). Reduction of this coupling by *sla2* deletion should have two effects. First, it should reduce the force opposing actin polymerization. Second, it should lead to less deformation and tension in the membrane. As discussed above (mechanisms *B2* and *B3* in Fig. 1), regulator detachment may be accelerated by tension. Therefore, *sla2* deletion could reduce detachment of regulators from the membrane, leading to a reduction in α. We reduce f_a by 90% (a nonzero force is needed to keep the actin gel near the membrane), and reduce α by varying amounts. Reductions <30% give actin pulses. Reductions >30% cause persistent and increased actin accumulation (see

Figs. 4 *d* and 5 *b* for a reduction of 90%). This reproduces the finding of persistent comet-shaped accumulations of actin in the *sla2* mutant (9,10). The fact that the reduction in α is needed to reproduce the actin comets suggests that the negative-feedback interaction is tension-dependent.

Latrunculin treatment. We model latrunculin treatment by setting $k_{on} = k_{br} = 0$, which equates to no actin polymerization. The regulator time course in Fig. 5 *b* shows that the regulator count goes to its maximal value and remains there. This is consistent with the observation that latrunculin greatly lengthens the lifetime of coat proteins and regulators (9).

Rate-equation models

Mathematical form. The rate-equation models abstract the essential ingredients of the more complex simulations, allow us to ascertain the robustness of the predictions, and facilitate more complete fitting of the models to the data. They treat the variables F (F-actin) and L (regulator Las17). For simplicity, we treat actin polymerization as a one-step process where a nucleator produces an actin filament that grows instantaneously to its final length. This approximation will be valid if the time it takes to grow a filament is shorter than the timescale of the endocytic dynamics. To estimate the filament growth time, we note that the free actin concentration is at the micromolar level (34). Assuming a value of 2 μM, and taking the actin polymerization rate to be 11.6 subunits s^{-1} μM^{-1} (64), we find that a typical actin filament of ~40 subunits (34) takes ~2 s to grow to its final length. By comparison, the actin lifetime in the patch is ~10 s. Therefore, regarding filament growth as instantaneous appears to be a reasonably good approximation. We have confirmed this by studying a four-variable model in which filament nucleation and growth are treated separately (see the Supporting Material). We find that the two-variable and four-variable models agree well, provided that the detachment rate parameter α in the four-variable model is reduced by ~10% relative to the two-variable model.

We implement our assumptions as follows:

$$\frac{dL}{dt} = k_0 L^2 (L_2 - L) - \alpha k_{br} L F, \tag{2}$$

$$\frac{dF}{dt} = k_{br} \bar{l} L F - k_{sev} F, \tag{3}$$

where k_{br} is the branching rate per subunit, $\bar{l}$ is the average filament length, α is the detachment probability for L per branching event, and k_{sev} is the disassembly rate of F. The first term in dL/dt is the same as the average assembly rate in the stochastic simulations. In this model the number of filaments N is $F/\bar{l}$. The second term is a nucleation rate of $k_{br}LF$, corresponding to autocatalytic branching. The first term in dF/dt combines the nucleation rate of $k_{br}LF$ with our assumption that filaments grow rapidly to length $\bar{l}$. Finally, the last term describes a simple first-order decay of F.

This model is similar to the classic Fitzhugh-Nagumo (FN) model (65,66), in that it has a nonlinear positive-feedback term driving assembly of the activator L, and an inhibitor F whose buildup drives the activator down (to be precise, $-F$ corresponds to the inhibitor in the FN model). However, the mathematical forms differ in three ways: 1) The buildup at small L is quadratic in L rather than linear as in the FN model, to reproduce the slow initial buildup of L (6,14); 2) the second term in dL/dt contains an added factor of L to prevent L from going negative; and 3) the first term of dF/dt contains an extra factor of F to account for autocatalytic branching.

Fitting and predictions of the two-variable model. The four adjustable parameters (k_0, k_{br}, k_{sev}, and α) are optimized to fit data for wild-type cells, while $\bar{l}$ was given a plausible value of 30 (any change in $\bar{l}$ could be compensated by making appropriate changes in α and k_{br}). We use a least-squares objective function to minimize the difference between the time courses given by the model and those obtained from experiment (see the Supporting Material). The value of L_2 is chosen to be the same as in the stochastic simulations. We choose $F = 1$ at the beginning of the simulation, as a starting point for autocatalytic growth. We find that our results are not sensitive to the value of L_0, and as in the stochastic simulations we used a value that is much smaller than L_2, but guarantees a large critical nucleus. The fit parameters are given in Table 1. Note that k_{br} is smaller than in the stochastic simulations because in this model all subunits are implicitly allowed to branch, while in the stochastic simulations only those near the membrane can branch. As seen in Fig. 6, the model matches the data reasonably well. The peak heights and full widths at half maximum of both F and L are reproduced well, as well as the slow buildup of L.

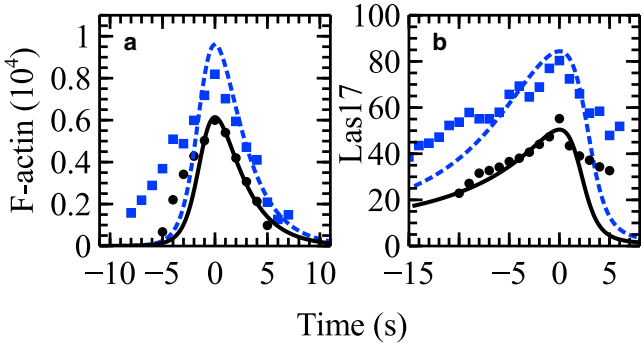

FIGURE 6 Rate-equation model with branching nucleation. Predicted time courses (*solid* and *dashed lines*) of (*a*) F and (*b*) L for wild-type (*black*) and *las17*Δ*acidic pan1*Δ*acidic* (*blue*) cells compared with experimental time courses (*dots*). F is the measured Abp1 count multiplied by a conversion factor of 8.9 (see text). For clarity, the error bars for the experimental data are not indicated here, but they are given in Fig. 5 *a*. To see this figure in color, go online.

We have predicted the effects of the same interventions, except for the *sla2* mutation, treated above by the stochastic-growth models. We used the same percent changes in the parameter values. We were unable to model the *sla2* deletion mutation in a physically reasonable fashion because the rate-equation model does not include opposing force.

The results (Fig. 6 and Table 2) are generally similar to the stochastic-growth model predictions. Under acidic-domain and actin disassembly mutations, both F_{max} and L_{max} increase substantially. Under latrunculin treatment, $F_{max} = 0$ but L climbs to an asymptotic value of L_2.

These results are fairly insensitive to the values of the unknown parameters L_0 and L_2. Reducing L_0 by 50% has no effect on the quality of fit in the wild-type case; increasing it by 50% increases the root-mean-square error by 10%. The sign of the phenotypic predictions made above is preserved, although their magnitude changes. Doubling L_2 increases the root-mean-square error of fit by 30%, but again leaves the qualitative predictions of the model unchanged.

Experimental Results

The data are given in Fig. 7. The time courses are aligned with each one having its maximum at time $t = 0$. They are truncated in time because the fractional error at smaller protein counts becomes large. The time courses of Abp1, Las17, and Myo5 reproduce the general features of those given in Sun et al. (14) and Picco et al. (6), including the slow buildup of Las17. Our wild-type peak values for Las17 and Myo5 (55 and 130) are similar to the values (43 and 130) measured for budding yeast in Picco et al. (6). They are, however, much smaller than the counts of the corresponding proteins Wsp1 and Myo1 (230 and 400) measured for fission yeast actin patches in Sirotkin et al. (67).

Abp1 count depends counterintuitively upon acidic-domain mutations

Fig. 7 *b* shows time courses of Abp1, our F-actin surrogate, in wild type and various Δ*acidic* mutants. The results are reasonably consistent with our previous ones (11), with the wild-type count being ~15% below the previous count and that for the *las17*Δ*acidic pan1*Δ*acidic* mutant being ~30% lower. The Abp1 counts in the *las17*Δ*acidic pan1*Δ*acidic* and *las17*Δ*acidic* mutants are larger than in the wild-type cells, by 37 and 20%, respectively, an effect similar to that found in our previous work. This is consistent with the predictions of both the stochastic (Fig. 5 *a*) and rate-equation (Fig. 6 *a*) models. On the other hand, the Abp1 count in the *myo3*Δ*acidic myo5*Δ*acidic pan1*Δ*acidic* and *myo3*Δ*acidic myo5*Δ*acidic* mutants is nearly equal to that in wild-type cells. The Δ*acidic* mutants that include the *pan1*Δ*acidic* mutation affect the Abp1 count more than those without the Pan1 mutation, but *pan1*Δ*acidic* itself has an almost negligible effect.

TABLE 2 Summary of Predictions of Rate-Equation Model

Phenotype	F_{max}	L_{max}
Wild-type	6133	50
*las17*Δacidic pan1Δacidic	9602	84
Actin disassembly mutation	8549	50
Latrunculin treatment	0	101

Acidic-domain mutation of Las17 increases Las17 count

Fig. 7 *c* shows that the Las17 count increases because of *las17*Δ*acidic* mutation. This is consistent with the predictions of both of the mathematical models (Figs. 5 *a* and 6 *b*). The peak height is increased by 55% in the *las17*Δ*acidic* mutant, and 60% in the *las17*Δ*acidic pan1*Δ*acidic* mutant. Thus the effect of the additional Pan1 mutation is small. The Las17 lifetime is increased in both these mutants. On the other hand, the Las17 count is essentially unaffected by mutations of Myo3 and Myo5, even when they are combined with mutations of Pan1.

Acidic-domain mutation of Myo5 increases Myo5 count

For Myo5, the largest effect is seen in the *myo3*Δ*acidic myo5*Δ*acidic pan1*Δ*acidic* mutant (see Fig. 7 *d*). The Myo5 peak height is increased by 120% in the mutant cells. Our models do not treat Myo5 explicitly, but the negative-feedback effect seen in Figs. 5 *a* and 6 *b* may contribute to the effect seen here. The effect requires the *pan1*Δ*acidic* mutation; the peak height is essentially unchanged in the *myo3*Δ*acidic myo5*Δ*acidic* mutant. The requirement for the *pan1*Δ*acidic* mutation in the case of Myo5 might result from the binding of Pan1 to Myo5 (68), but we do not know precisely how this binding would affect the Myo5 count. The lifetime is also increased in the *myo3*Δ*acidic myo5*Δ*acidic pan1*Δ*acidic* and *myo3*Δ*acidic myo5*Δ*acidic* mutants. The Myo5 count is affected much less by mutations in Las17 and Pan1. The Myo3 count is generally less sensitive to mutations than the Myo5 count. We do not know the reason for this difference. However, we are not aware of in vitro measurements of the nucleation activity of Myo3, so it is possible that Myo3 is a weaker nucleator than Myo5.

Acidic-domain mutation of Pan1 extends Pan1 lifetime

For Pan1, the peak height is not significantly changed by any of the mutations. However, its lifetime is dramatically increased in the *las17*Δ*acidic pan1*Δ*acidic* mutant. Treating this effect within our theoretical framework would require the inclusion of multiple regulators, which is beyond the scope of this article.

DISCUSSION

We have tested a negative-feedback mechanism for protein dynamics at endocytic actin patches in budding yeast,

using both stochastic-growth simulations and rate-equation models. Both of these models reproduce the pulse nature of the protein time courses. In addition, these models predict (Figs. 5 *a* and 6 *b*) that the maximum counts of Arp2/3 regulators will be increased by mutations that reduce the regulators' activity. We tested the robustness of the prediction by varying key assumptions (see the Supporting Material) and found the prediction to be robust to these variations.

The physical mechanism is the following: branching and concomitant actin polymerization increase the probability for Arp2/3 regulators to leave the membrane, either by being directly pulled off with the nascent branch or via mechanical effects. Therefore, reducing branching/actin polymerization increases the fraction of regulators left on the membrane. The prediction was confirmed in vivo by analyzing movies of CME in live cells to evaluate the time courses of the regulators, in wild-type cells and cells with mutated Arp2/3-binding domains. Large increases in the counts were seen for Las17 and Myo5, the regulators having the strongest branching activity (Fig. 7, *c* and *d*).

Another mechanism that might explain the increased Arp2/3 regulator counts is that the mutations reduce the strength of the binding between Arp2/3 complex and the regulators. This corresponds to reducing the parameter α in our models, which determines the rate of regulator detachment. We have implemented this hypothesis, and find that it can match the increase in Arp2/3 regulator peak height, but it greatly overestimates the increase in the F-actin peak height. Therefore, we feel that the negative-feedback mechanism based on the branching rate is a more likely explanation.

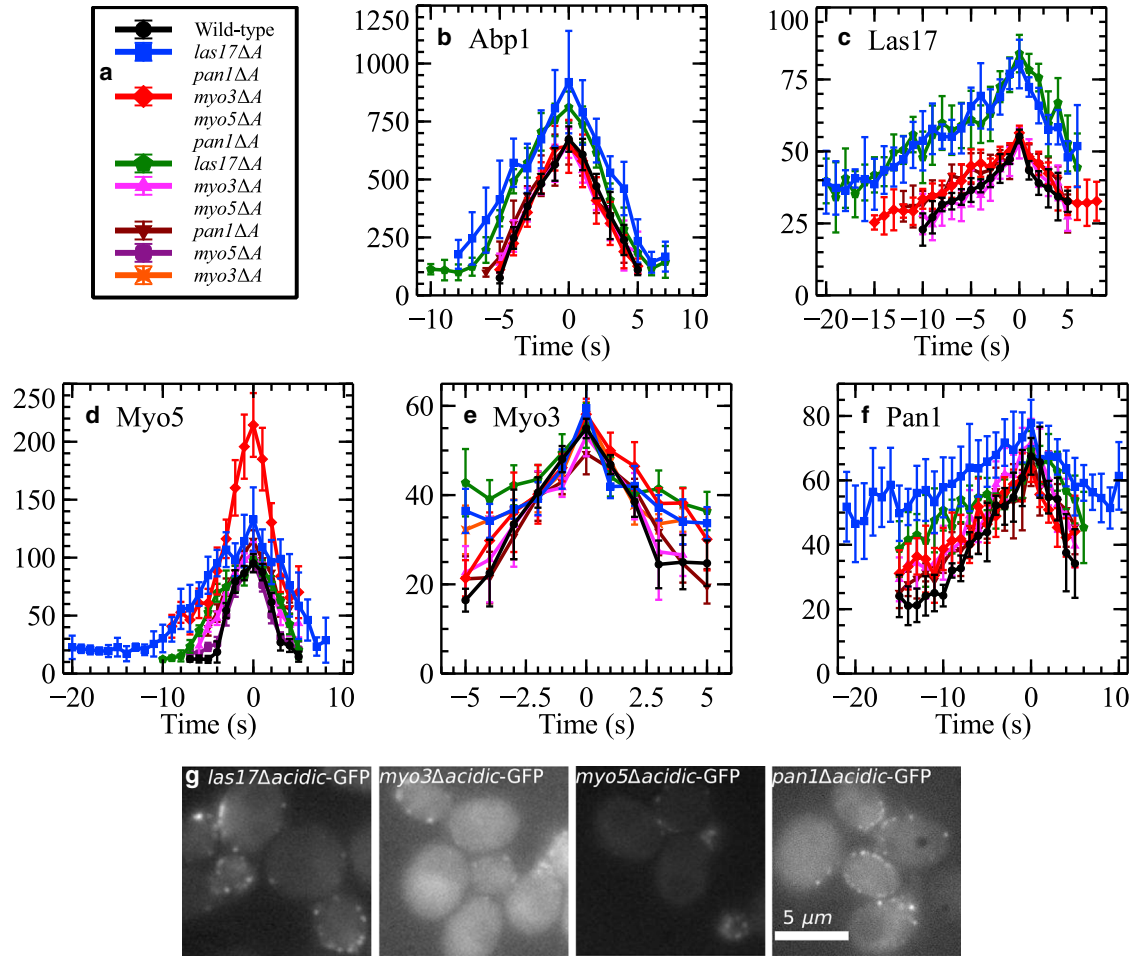

FIGURE 7 (*a*) Measured time courses of (*b*) Abp1, (*c*) Las17, (*d*) Myo5, (*e*) Myo3, and (*f*) Pan1 for wild-type cells and several mutants. Δ*A* in the legend means Δ*acidic*. Numbers of patches measured (*N*) in Abp1-GFP are $N = 184$, 132, 148, 274, 64, and 331, for wild-type, *las17*Δ*Apan1*Δ*A*, *myo3*Δ*Amyo5*Δ*Apan1*Δ*A*, *las17*Δ*A*, *myo3*Δ*Amyo5*Δ*A*, and *pan1*Δ*A*, respectively. Following the same order, in Las17-GFP, $N = 197$, 202, 181, 151, 88, and 202. In Myo5-GFP, $N = 279$, 90, 677, 366, 517, and 491. In Myo3-GFP, $N = 307$, 437, 601, 161, 159, 187, and 627. In Pan1-GFP, $N = 206$, 263, 183, 347, 151, and 96. In addition, for Myo5-GFP *myo5*Δ*A*, $N = 1070$. Plotted points correspond to mode values; error bars are the standard deviation of a distribution of mode values obtained by bootstrapping (see the Supporting Material). Frame (*g*) shows representative fluorescence images of GFP-labeled regulators. To see this figure in color, go online.

The negative-feedback models can also explain the increased F-actin peak height caused by some acidic-domain mutations (Fig. 7 *b*). What other mechanisms might explain this observation?

1) If actin assembly at endocytic actin patches were diffusion-limited, i.e., every actin monomer that contacts the patch region is polymerized, then reducing k_{br} would not decrease F_{max}. However, this assumption is not likely to hold. If one considers the actin patch as a spherical perfect absorber of radius $R = 100$ nm (7), assumes a diffusion coefficient of $D = 5\ \mu M^2$ for monomeric actin (69), and takes a monomeric actin concentration of $C = 2\ \mu M$, one obtains a diffusion-limited monomer flux (70) of $4\pi DCR = 7500$ monomers/s. This is considerably greater than our maximum measured actin assembly rate of 900 monomers/s obtained by multiplying the maximum slope of Fig. 7 *b* by a conversion factor of 8.9 to obtain the F-actin assembly rate. In addition, the diffusion-limiting hypothesis does not explain our measured increase of both F-actin and regulator peak height.
2) Weakened regulator-Arp2/3 binding caused by acidic-domain mutations could enhance Arp2/3 release from the regulators bound to the membrane. This could explain the F-actin results in two ways. First, release of Arp2/3 complex from regulators has been shown to accelerate branch formation (25). Second, enhanced Arp2/3 release could accelerate polymerization by reducing the force opposing actin polymerization. Finally, as mentioned above, weakening of the regulator-Arp2/3 binding could cause fewer regulators to detach from the membrane. We again treated this effect by reducing α. As mentioned above, the predictions fit the data poorly.

Thus we feel that the negative-feedback hypothesis is the most likely explanation of this observation. Because the model with negative feedback driven entirely by membrane tension (mechanisms *B2* and *B3* in Fig. 1 and Supporting Material) did not fit the data, the negative feedback interaction must depend to some extent on branching (mechanism *B1*). Another observation supporting mechanism *B1* is that the regulators assemble almost independently. Fig. 7, *c* and *d*, shows that acidic-domain mutation of one particular regulator affects that same regulator most strongly, with relatively weak effects on the other regulators. This argues against mechanisms *B2* and *B3* being dominant. These mechanisms would predict that mutation of Las17 would affect Las17 and Myo3/5 roughly equally, because they are both at the base of the invagination (6). Only mechanism *B1*, where individual branching events lead to regulator detachment, would lead to the observed independent assembly of the regulators. On the other hand, we found that reproducing the actin comets in *sla2* deletion mutants required a mechanical coupling in the negative feedback term. A likely explanation of these findings is that detachment of regulators from the membrane is driven by branch formation, with a rate depending on force. This could be included by generalizing our model to have a deformation-dependent α. Such a model would have additional fitting parameters, and in the absence of more detailed information about the mechanochemical couplings, we did not pursue this approach.

Another key assumption of our model is that of autocatalytic Las17 assembly, independent of F-actin. An alternate hypothesis is that Las17 assembly passively follows the assembly of an upstream factor in the endocytic patch. Kaksonen et al. (5) showed that mutation of clathrin, which acts upstream of Las17, reduces the Las17 lifetime. This suggests that clathrin aids Las17 assembly. But the very different time courses of Las17 and clathrin argue against Las17 following clathrin passively. Clathrin may instead act as a platform for autocatalytic Las17 assembly. Bzz1 has also been found to activate the fission yeast Las17 analog Wsp1 (71). Our assembly dynamics could describe this system, provided that Wsp1 is assumed to assemble in a background containing Bzz1. The autocatalytic Las17 assembly hypothesis could be tested by measuring the effects of more upstream proteins, such as Bzz1, on Las17 assembly.

Despite the large evolutionary distance between budding yeast and fission yeast, the need to overcome a large turgor pressure in both organisms may have led to some commonality in their endocytic machineries. Thus, the basic mechanisms studied here for budding yeast may also be relevant to fission yeast. A major difference between the two systems is the larger counts of most of the patch constituents in fission yeast (19,67) versus budding yeast (6,11,61). In our model, a multiplication of all time courses by, for example, a factor of two could be obtained by the following adjustments: 1) doubling L_0, L_2, f_a, and the starting number of actin filaments; and 2) reducing k_{br} by 50% and k_0 by 75%. This system would generate twice as much force. Thus, the higher protein counts in fission yeast may help overcome the higher turgor pressure in this system relative to budding yeast.

Another difference between budding yeast and fission yeast is the larger inward motion of Wsp1 in fission yeast (67) (nearly 300 nm). This suggests that a substantial fraction of the Wsp1 1) incorporates into the actin network, or 2) moves up the sides of the tubule. If 1) holds, and Wsp1 in the network continues to activate Arp2/3 complex, the negative-feedback mechanism treated here could be weaker. If 2) holds, actin polymerization will exert forces perpendicular to the sides of the tubule, which will compress it, and thus aid the scission process. However, less force would be available for pulling the invagination into the cytoplasm. Finally, the time course of Wsp1 (67) has a faster assembly period than that for Las17.

We do not know how modifying the model to treat fission yeast would change the results. However, the negative-feedback interaction explored here may be relevant to several

findings regarding fission yeast: 1) Treatment with CK-666, which inhibits Arp2/3-based branching, was found to give nearly unchanged F_{max} values (8). In a model without negative feedback, a large drop in F_{max} would have occurred. 2) Mutation of cofilin gave actin patches that were brighter by 10–70% (8,19), similar to our predictions for budding yeast (Fig. 5 *b*).

Could the model predictions made here be reproduced by previous models in the literature? Berro et al. (13) treated a feedforward model of endocytosis in fission yeast using a pulse of active WASP (corresponding to L in our calculations) with a fixed magnitude and time dependence. This model treats branching using several steps, but our k_{br} would correspond most closely to the activation rate of Arp2/3 bound to a filament. Reducing this rate by 40% would cause a large reduction in F_{max}, unlike the increase seen in our data and models. Furthermore, L_{max} would be unchanged, because a fixed pulse height and shape were assumed. Therefore the model of Berro et al. (13) would require substantial modification to reproduce our predictions and experimental findings.

Berro et al. (13) also reported a number of uncapped filaments $N_u \simeq 8$. In contrast, we find that $N_u \simeq 140$. We believe the discrepancy arises because Berro et al. (13) did not treat the effects of opposing force on the growing filaments. If we multiply the on-rate assumed in Berro et al. (13) by a factor of $\exp(-f_a\delta/N_u k_B T)$, the value of N_u required to match the maximum polymerization rate of 2000 s^{-1} (13) increases. For $f_a = 415$pN, as above, this approach gives $N_u = 101$.

The model of Liu et al. (12) for budding yeast includes the following chain of feedback interactions of polymerized actin onto membrane-bound agents that act upstream of actin nucleation: $F \rightarrow$ membrane bending $\rightarrow$ coat protein turnover, as well as another chain including PIP2 hydrolysis. The net result of each of these chains is that F feeds back negatively on the coat proteins C. The model did not treat actin regulators explicitly. However, if the regulators were taken to be included in C, and k_{br} were to be identified with the rate constant k_7 (Eq. 4 of Liu et al. (12)) coupling C to actin assembly, a reduction in k_7 could lead to an increase in C_{max}, paralleling the increase in L_{max} that we have predicted and observed. It is not clear whether this could lead to an increase in F_{max}, because this requires the increase in C_{max} to overcome the direct effect of decreasing k_7.

A major difference between this model and that of Liu et al. (12) is in the assumed distribution of actin polymerization. Liu et al. (12) assumes actin polymerization focused on the invagination, while we take it to be focused in a disklike region around the invagination. Our assumption is based on explicit mechanical calculations (40) showing that a disklike distribution can lead to a density of pulling force much greater than the polymerization stall stress. We are not aware of calculations showing that polymerization in the bud region can produce pulling forces. The merits of the differing assumptions about the distribution of actin polymerization could be directly evaluated via superresolution measurements of the distribution of regulators.

The mathematical similarity between our models and those used previously to treat F-actin waves in mammalian cells (reviewed in Allard and Mogilner (23)) suggests similarities between endocytosis and F-actin waves. They are, indeed, parallel in several aspects. As in the case of endocytosis, actin regulators (WAVE complex) and Type-1 myosins (Myosin 1B) in actin waves precede F-actin (72,73). In both processes, phosphoinositides enhance actin polymerization (74). Finally, Cdc42 waves, which should correspond to F-actin waves, are closely coupled to clathrin waves (75), which could drive waves of endocytosis. Thus, these two phenomena may be variants of the same process.

The negative-feedback interaction studied here may be a generic component of the circuits by which the cell controls actin dynamics at the membrane. It provides a natural mechanism for generating a burst of actin polymerization where needed. It also prevents excessive local F-actin buildup that could otherwise result from autocatalytic branching polymerization. Finally, it could act as a homeostatic mechanism protecting actin assembly against perturbations. A robust finding of our models is that large changes in key rates, such as those of branching and severing, have surprisingly modest effects on the peak F-actin count.

SUPPORTING MATERIAL

Supporting Materials and Methods, five figures, and two tables are available at http://www.biophysj.org/biophysj/supplemental/S0006-3495(16)00164-8.

AUTHOR CONTRIBUTIONS

X.W. analyzed the fluorescence videos, collaborated on developing the theoretical models, and performed the model calculations; B.J.G. prepared the yeast strains and performed the experiments; J.A.C. supervised the experiments and collaborated on data analysis; A.E.C. collaborated on developing the theoretical models and analyzing the fluorescence videos, and supervised the model calculations; and the article was written by X.W. and A.E.C. and modified by B.J.G. and J.A.C.

ACKNOWLEDGMENTS

Megan Cohan and Stefanie Shahan helped in the development of the tracking methodology. We appreciate informative conversations with David Kovar.

This work was supported by the National Institutes of Health under grants No. R01 GM107667, R01 GM086882, R01 GM38542, and R01 GM95509.

SUPPORTING CITATIONS

References (76-82) appear in the Supporting Material.

REFERENCES

1. McMahon, H. T., and E. Boucrot. 2011. Molecular mechanism and physiological functions of clathrin-mediated endocytosis. *Nat. Rev. Mol. Cell Biol.* 12:517–533.
2. Weinberg, J., and D. G. Drubin. 2012. Clathrin-mediated endocytosis in budding yeast. *Trends Cell Biol.* 22:1–13.
3. Mooren, O. L., B. J. Galletta, and J. A. Cooper. 2012. Roles for actin assembly in endocytosis. *Annu. Rev. Biochem.* 81:661–686.
4. Boulant, S., C. Kural, …, T. Kirchhausen. 2011. Actin dynamics counteract membrane tension during clathrin-mediated endocytosis. *Nat. Cell Biol.* 13:1124–1131.
5. Kaksonen, M., C. P. Toret, and D. G. Drubin. 2005. A modular design for the clathrin- and actin-mediated endocytosis machinery. *Cell.* 123:305–320.
6. Picco, A., M. Mund, …, M. Kaksonen. 2015. Visualizing the functional architecture of the endocytic machinery. *eLife.* 4:e04535.
7. Kukulski, W., M. Schorb, …, J. A. Briggs. 2012. Plasma membrane reshaping during endocytosis is revealed by time-resolved electron tomography. *Cell.* 150:508–520.
8. Burke, T. A., J. R. Christensen, …, D. R. Kovar. 2014. Homeostatic actin cytoskeleton networks are regulated by assembly factor competition for monomers. *Curr. Biol.* 24:579–585.
9. Kaksonen, M., Y. Sun, and D. G. Drubin. 2003. A pathway for association of receptors, adaptors, and actin during endocytic internalization. *Cell.* 115:475–487.
10. Skruzny, M., T. Brach, …, M. Kaksonen. 2012. Molecular basis for coupling the plasma membrane to the actin cytoskeleton during clathrin-mediated endocytosis. *Proc. Natl. Acad. Sci. USA.* 109:E2533–E2542.
11. Galletta, B. J., A. E. Carlsson, and J. A. Cooper. 2012. Molecular analysis of Arp2/3 complex activation in cells. *Biophys. J.* 103:2145–2156.
12. Liu, J., Y. Sun, …, G. F. Oster. 2009. The mechanochemistry of endocytosis. *PLoS Biol.* 7:e1000204.
13. Berro, J., V. Sirotkin, and T. D. Pollard. 2010. Mathematical modeling of endocytic actin patch kinetics in fission yeast: disassembly requires release of actin filament fragments. *Mol. Biol. Cell.* 21:2905–2915.
14. Sun, Y., A. C. Martin, and D. G. Drubin. 2006. Endocytic internalization in budding yeast requires coordinated actin nucleation and myosin motor activity. *Dev. Cell.* 11:33–46.
15. Li, P., S. Banjade, …, M. K. Rosen. 2012. Phase transitions in the assembly of multivalent signalling proteins. *Nature.* 483:336–340.
16. Banjade, S., and M. K. Rosen. 2014. Phase transitions of multivalent proteins can promote clustering of membrane receptors. *eLife.* 3:e04123.
17. Madania, A., P. Dumoulin, …, B. Winsor. 1999. The *Saccharomyces cerevisiae* homologue of human Wiskott-Aldrich syndrome protein Las17p interacts with the Arp2/3 complex. *Mol. Biol. Cell.* 10:3521–3538.
18. Basu, R., and F. Chang. 2011. Characterization of dip1p reveals a switch in Arp2/3-dependent actin assembly for fission yeast endocytosis. *Curr. Biol.* 21:905–916.
19. Chen, Q., and T. D. Pollard. 2013. Actin filament severing by cofilin dismantles actin patches and produces mother filaments for new patches. *Curr. Biol.* 23:1154–1162.
20. Basu, R., E. L. Munteanu, and F. Chang. 2014. Role of turgor pressure in endocytosis in fission yeast. *Mol. Biol. Cell.* 25:679–687.
21. Weiner, O. D., W. A. Marganski, …, M. W. Kirschner. 2007. An actin-based wave generator organizes cell motility. *PLoS Biol.* 5:e221.
22. Millius, A., N. Watanabe, and O. D. Weiner. 2012. Diffusion, capture and recycling of SCAR/WAVE and Arp2/3 complexes observed in cells by single-molecule imaging. *J. Cell Sci.* 125:1165–1176.
23. Allard, J., and A. Mogilner. 2013. Traveling waves in actin dynamics and cell motility. *Curr. Opin. Cell Biol.* 25:107–115.
24. Co, C., D. T. Wong, …, J. Taunton. 2007. Mechanism of actin network attachment to moving membranes: barbed end capture by N-WASP WH2 domains. *Cell.* 128:901–913.
25. Smith, B. A., S. B. Padrick, …, J. Gelles. 2013. Three-color single molecule imaging shows WASP detachment from Arp2/3 complex triggers actin filament branch formation. *eLife.* 2:e01008.
26. Urbanek, A. N., A. P. Smith, …, K. R. Ayscough. 2013. A novel actin-binding motif in Las17/WASP nucleates actin filaments independently of Arp2/3. *Curr. Biol.* 23:196–203.
27. Saleem, M., S. Morlot, …, A. Roux. 2015. A balance between membrane elasticity and polymerization energy sets the shape of spherical clathrin coats. *Nat. Commun.* 6:6249.
28. Tsujita, K., T. Takenawa, and T. Itoh. 2015. Feedback regulation between plasma membrane tension and membrane-bending proteins organizes cell polarity during leading edge formation. *Nat. Cell Biol.* 17:749–758.
29. Takano, K., K. Toyooka, and S. Suetsugu. 2008. EFC/F-BAR proteins and the N-WASP-WIP complex induce membrane curvature-dependent actin polymerization. *EMBO J.* 27:2817–2828.
30. Sun, Y., S. Carroll, …, D. G. Drubin. 2007. PtdIns(4,5)P2 turnover is required for multiple stages during clathrin- and actin-dependent endocytic internalization. *J. Cell Biol.* 177:355–367.
31. Stefan, C. J., S. M. Padilla, …, S. D. Emr. 2005. The phosphoinositide phosphatase Sjl2 is recruited to cortical actin patches in the control of vesicle formation and fission during endocytosis. *Mol. Cell. Biol.* 25:2910–2923.
32. Ahyayauch, H., A. V. Villar, …, F. M. Goñi. 2005. Modulation of PI-specific phospholipase C by membrane curvature and molecular order. *Biochemistry.* 44:11592–11600.
33. Pollard, T. D., and G. G. Borisy. 2003. Cellular motility driven by assembly and disassembly of actin filaments. *Cell.* 112:453–465.
34. Goode, B. L., J. A. Eskin, and B. Wendland. 2015. Actin and endocytosis in budding yeast. *Genetics.* 199:315–358.
35. Carlsson, A. E. 2010. Dendritic actin filament nucleation causes traveling waves and patches. *Phys. Rev. Lett.* 104:228102.
36. Doubrovinski, K., and K. Kruse. 2008. Cytoskeletal waves in the absence of molecular motors. *Europhys. Lett.* 83:18003.
37. Holmes, W. R., A. E. Carlsson, and L. Edelstein-Keshet. 2012. Regimes of wave type patterning driven by refractory actin feedback: transition from static polarization to dynamic wave behaviour. *Phys. Biol.* 9:046005.
38. Ryan, G. L., H. M. Petroccia, …, D. Vavylonis. 2012. Excitable actin dynamics in lamellipodial protrusion and retraction. *Biophys. J.* 102:1493–1502.
39. Carlsson, A. E. 2001. Growth of branched actin networks against obstacles. *Biophys. J.* 81:1907–1923.
40. Carlsson, A. E., and P. V. Bayly. 2014. Force generation by endocytic actin patches in budding yeast. *Biophys. J.* 106:1596–1606.
41. Kaksonen, M., C. P. Toret, and D. G. Drubin. 2006. Harnessing actin dynamics for clathrin-mediated endocytosis. *Nat. Rev. Mol. Cell Biol.* 7:404–414.
42. Galletta, B. J., and J. A. Cooper. 2009. Actin and endocytosis: mechanisms and phylogeny. *Curr. Opin. Cell Biol.* 21:20–27.
43. Li, D., L. Shao, …, E. Betzig. 2015. Extended-resolution structured illumination imaging of endocytic and cytoskeletal dynamics. *Science.* 349:aab3500.
44. Idrissi, F.-Z., H. Grötsch, …, M. I. Geli. 2008. Distinct acto/myosin-I structures associate with endocytic profiles at the plasma membrane. *J. Cell Biol.* 180:1219–1232.
45. Weisswange, I., T. P. Newsome, …, M. Way. 2009. The rate of N-WASP exchange limits the extent of ARP2/3-complex-dependent actin-based motility. *Nature.* 458:87–91.
46. Avinoam, O., M. Schorb, …, M. Kaksonen. 2015. Endocytic sites mature by continuous bending and remodeling of the clathrin coat. *Science.* 348:1369–1372.

47. Duffy, G. H. 1962. Physical Chemistry. McGraw Hill, New York.
48. Aghamohammadzadeh, S., and K. R. Ayscough. 2009. Differential requirements for actin during yeast and mammalian endocytosis. *Nat. Cell Biol.* 11:1039–1042.
49. Martinez de Marañon, I., P. A. Marechal, and P. Gervais. 1996. Passive response of *Saccharomyces cerevisiae* to osmotic shifts: cell volume variations depending on the physiological state. *Biochem. Biophys. Res. Commun.* 227:519–523.
50. Schaber, J., M. À. Adrover, …, E. Klipp. 2010. Biophysical properties of *Saccharomyces cerevisiae* and their relationship with HOG pathway activation. *Eur. Biophys. J.* 39:1547–1556.
51. Minc, N., A. Boudaoud, and F. Chang. 2009. Mechanical forces of fission yeast growth. *Curr. Biol.* 19:1096–1101.
52. Peskin, C. S., G. M. Odell, and G. F. Oster. 1993. Cellular motions and thermal fluctuations: the Brownian ratchet. *Biophys. J.* 65:316–324.
53. https://developer.nvidia.com/cuda-toolkit.
54. Achard, V., J.-L. Martiel, …, R. Boujemaa-Paterski. 2010. A "primer"-based mechanism underlies branched actin filament network formation and motility. *Curr. Biol.* 20:423–428.
55. Collins, A., A. Warrington, …, T. Svitkina. 2011. Structural organization of the actin cytoskeleton at sites of clathrin-mediated endocytosis. *Curr. Biol.* 21:1167–1175.
56. Winter, D., T. Lechler, and R. Li. 1999. Activation of the yeast Arp2/3 complex by Bee1p, a WASP-family protein. *Curr. Biol.* 9:501–504.
57. Rohatgi, R., L. Ma, …, M. W. Kirschner. 1999. The interaction between N-WASP and the Arp2/3 complex links Cdc42-dependent signals to actin assembly. *Cell.* 97:221–231.
58. Wen, K.-K., and P. A. Rubenstein. 2005. Acceleration of yeast actin polymerization by yeast Arp2/3 complex does not require an Arp2/3-activating protein. *J. Biol. Chem.* 280:24168–24174.
59. Okreglak, V., and D. G. Drubin. 2007. Cofilin recruitment and function during actin-mediated endocytosis dictated by actin nucleotide state. *J. Cell Biol.* 178:1251–1264.
60. Belmont, L. D., and D. G. Drubin. 1998. The yeast V159N actin mutant reveals roles for actin dynamics in vivo. *J. Cell Biol.* 142:1289–1299.
61. Lin, M.-C., B. J. Galletta, …, J. A. Cooper. 2010. Overlapping and distinct functions for cofilin, coronin and Aip1 in actin dynamics in vivo. *J. Cell Sci.* 123:1329–1342.
62. Lappalainen, P., and D. G. Drubin. 1997. Cofilin promotes rapid actin filament turnover in vivo. *Nature.* 388:78–82.
63. Skruzny, M., A. Desfosses, …, M. Kaksonen. 2015. An organized co-assembly of clathrin adaptors is essential for endocytosis. *Dev. Cell.* 33:150–162.
64. Pollard, T. D. 1986. Rate constants for the reactions of ATP- and ADP-actin with the ends of actin filaments. *J. Cell Biol.* 103:2747–2754.
65. Fitzhugh, R. 1961. Impulses and physiological states in theoretical models of nerve membrane. *Biophys. J.* 1:445–466.
66. Nagumo, J., S. Arimoto, and S. Yoshizawa. 1962. An active pulse transmission line simulating nerve axon. *Proc. IRE.* 50:2061–2070.
67. Sirotkin, V., J. Berro, …, T. D. Pollard. 2010. Quantitative analysis of the mechanism of endocytic actin patch assembly and disassembly in fission yeast. *Mol. Biol. Cell.* 21:2894–2904.
68. Barker, S. L., L. Lee, …, B. Wendland. 2007. Interaction of the endocytic scaffold protein Pan1 with the type I myosins contributes to the late stages of endocytosis. *Mol. Biol. Cell.* 18:2893–2903.
69. McGrath, J. L., Y. Tardy, …, J. H. Hartwig. 1998. Simultaneous measurements of actin filament turnover, filament fraction, and monomer diffusion in endothelial cells. *Biophys. J.* 75:2070–2078.
70. Berg, H. C. 1993. Random Walks in Biology. Princeton University Press, Princeton, NJ.
71. Arasada, R., and T. D. Pollard. 2011. Distinct roles for F-BAR proteins Cdc15p and Bzz1p in actin polymerization at sites of endocytosis in fission yeast. *Curr. Biol.* 21:1450–1459.
72. Lam Hui, K., S. I. Kwak, and A. Upadhyaya. 2014. Adhesion-dependent modulation of actin dynamics in Jurkat T cells. *Cytoskeleton (Hoboken).* 71:119–135.
73. Bretschneider, T., K. Anderson, …, G. Gerisch. 2009. The three-dimensional dynamics of actin waves, a model of cytoskeletal self-organization. *Biophys. J.* 96:2888–2900.
74. Gerisch, G., B. Schroth-Diez, …, M. Ecke. 2012. PIP3 waves and PTEN dynamics in the emergence of cell polarity. *Biophys. J.* 103:1170–1178.
75. Yang, Y., M. Su, and M. Wu. 2014. Visualizing collective dynamics of endocytic proteins. *American Society for Cell Biology 2014 Annual Meeting Abstracts, 2014.* 25:3987 (Abstract A1689).
76. Brachmann, C. B., A. Davies, …, J. D. Boeke. 1998. Designer deletion strains derived from *Saccharomyces cerevisiae* S288C: a useful set of strains and plasmids for PCR-mediated gene disruption and other applications. *Yeast.* 14:115–132.
77. Sheff, M. A., and K. S. Thorn. 2004. Optimized cassettes for fluorescent protein tagging in *Saccharomyces cerevisiae*. *Yeast.* 21:661–670.
78. Galletta, B. J., D. Y. Chuang, and J. A. Cooper. 2008. Distinct roles for Arp2/3 regulators in actin assembly and endocytosis. *PLoS Biol.* 6:e1.
79. Waddle, J. A., T. S. Karpova, …, J. A. Cooper. 1996. Movement of cortical actin patches in yeast. *J. Cell Biol.* 132:861–870.
80. Hiraoka, Y., J. W. Sedat, and D. A. Agard. 1990. Determination of three-dimensional imaging properties of a light microscope system. Partial confocal behavior in epifluorescence microscopy. *Biophys. J.* 57:325–333.
81. Hoffman, D. B., C. G. Pearson, …, E. D. Salmon. 2001. Microtubule-dependent changes in assembly of microtubule motor proteins and mitotic spindle checkpoint proteins at PtK1 kinetochores. *Mol. Biol. Cell.* 12:1995–2009.
82. Hedges, S. B., and P. Shah. 2003. Comparison of mode estimation methods and application in molecular clock analysis. *BMC Bioinformatics*. 4:31.